Quantum theory of plasmon–phonon scattering in multisubband systems

Journal of Physics: Condensed Matter

PAPER

Quantum theory of plasmon–phonon scattering in multisubband systems

Sofia Ribeiro[1,*] and Hugo Terças[2,3]

[1] Max Planck Institute for the Science of Light, Staudtstraße 2, D-91058 Erlangen, Germany
[2] Instituto Superior de Engenharia de Lisboa, Instituto Politécnico de Lisboa, Rua Conselheiro Emídio Navarro 1, Lisboa 1959-007, Portugal
[3] Instituto de Plasmas e Fusão Nuclear, Instituto Superior Técnico, Universidade de Lisboa, Av. Rovisco Pais 1, Lisboa 1049-001, Portugal
[*] Author to whom any correspondence should be addressed.

E-mail: sofia.ribeiro@mpl.mpg.de and hugo.tercas@isel.pt

Keywords: multisubband plasmons, phonons, scattering processes

OPEN ACCESS

RECEIVED
6 August 2025

REVISED
24 November 2025

ACCEPTED FOR PUBLICATION
10 December 2025

PUBLISHED
23 December 2025

Abstract

We present a first-principles quantum theory of a critical yet unexplored energy-loss pathway in low-dimensional semiconductors: resonant second-order scattering between multisubband (MSB) plasmons mediated by longitudinal optical phonons. Specifically, we demonstrate how a high-energy MSB plasmon decays into a lower-energy plasmon state via phonon emission—a fundamental process governing energy relaxation and decoherence in quantum wells. Through exact diagonalization of the coupled plasmon–phonon system and derivation of an effective Hamiltonian, we identify *density-tunable resonance conditions* that maximize scattering efficiency. Our numerical simulations for GaInAs quantum wells reveal scattering rates ($\sim 10\,\mathrm{ns}^{-1}$) competitive with radiative losses, with carrier density acting as a control knob. These results resolve the interplay of collective electronic and vibrational modes in confined systems, providing design principles to mitigate losses in infrared photodetectors, quantum cascade lasers, and plasmon-based quantum devices.

1. Introduction

The performance of many optoelectronic devices, such as quantum cascade lasers (QCLs) and infrared (IR) photodetectors, cannot be fully described by single-electron behavior alone; rather, it depends critically on the collective response of the charge carriers [1, 2]. Crucially, energy-relaxation pathways involving collective electronic modes fundamentally limit device speed and efficiency, yet a key dissipation channel—second-order inelastic scattering in which a high-energy multisubband (MSB) plasmon decays into a lower-energy plasmon via longitudinal optical (LO) phonon emission—remains poorly understood and unquantified. Over recent decades, collective excitations in a two-dimensional (2D) electron gas have been identified as key factors influencing the characteristic electronic frequencies [3, 4]. In particular, this collective response in quantum wells underpins the operation of light-emitting and light-detecting devices in the IR regime [5–8].

The interaction between intersubband (ISB) transitions and optical phonons plays a vital role in optoelectronic applications, as it governs the carrier lifetimes in excited subbands—an aspect that has been extensively studied [9–11]. For systems with high electron densities, electron–electron (Coulomb) interactions cannot be neglected. These interactions renormalize excitation energies, giving rise to a plasmon mode known as the ISB plasmon [1, 12], as schematically illustrated in the figures 1(a) and (b). Strong coupling between ISB plasmons and photons in a microcavity or between transverse optical phonon polaritons and ISB plasmons [13–17], has led to phenomena such as stimulated scattering and lasing. These processes typically involve relaxation from the upper to the lower polariton branch via LO-phonon scattering. Notably, [18] provided experimental evidence for scattering between ISB polaritons

and LO phonons, while [7, 8] explored the feasibility of ISB polariton lasers driven by optical pumping. These studies, however, have primarily focused on systems involving ISB polaritons and LO phonons.

In quantum wells with high doping levels and multiple occupied subbands, dipole–dipole interactions between ISB excitations significantly reshape the optical spectrum—this results in the emergence of MSB plasmons [19–23], see figures 1(c) and (d). MSB plasmons correspond to charge density waves that propagate in the plane of the quantum well, characterized by a specific in-plane wavevector; at high observation angles and elevated carrier densities, multiple MSB plasmon modes can be observed [24, 25]. With lifetimes on the order of a few femtoseconds, these collective excitations hold promise for efficient light emitters operating in the mid- and far-IR [23, 26]. This motivates a deeper investigation into the scattering processes in devices where MSB plasmons couple directly to free-space radiation [26, 27].

A microscopic quantum theory of MSB polarons—i.e., MSB excitations coupled to LO phonons—was recently proposed in [28]. The study demonstrated that the coupling strength between MSB transitions and LO phonons can be tuned from weak to strong, even reaching the ultra-strong coupling regime across various III-V and II-VI material systems. Building on this foundation, the present work aims to investigate how collective excitations in quantum wells affect energy relaxation times, which are typically governed by single-particle interactions. Our primary objective is to analyze the scattering of MSB plasmons by LO phonons—specifically, the process in which a higher-energy MSB plasmon decays into a lower-energy MSB state via the emission of an optical phonon. This MSB-phonon scattering process represents an important mechanism of energy exchange between collective electronic modes and lattice vibrations, with significant implications for quantum well-based technologies. A better understanding of this process can inform the design of IR detectors, QCLs, and other advanced optoelectronic devices by clarifying the underlying energy relaxation and loss mechanisms at the nanoscale.

In this work, we develop a microscopic quantum theory of stimulated scattering between MSB plasmons in a 2D electron gas, mediated by optical-phonon interactions. We specifically address the resonant process in which a high-energy MSB plasmon decays into a lower-energy plasmon state, accompanied by LO phonon emission—a critical yet unexplored energy-relaxation pathway in doped quantum wells. Building on the Hamiltonian for MSB plasmon–phonon coupling established in [28], in section 2, we derive a quantum-mechanical formulation of the effective second-order interaction governing phonon-mediated plasmon–plasmon scattering. In section 3, we solve the coupled equations of motion recursively by expanding the dynamics in the MSB plasmon field operator, extracting effective interaction Hamiltonians from each multi-plasmon process term. These results are applied to a GaInAs infinite quantum well model that incorporates realistic loss mechanisms to quantify the scattering efficiency. Concluding remarks and implications for device design are presented in the section 4.

2. Microscopic theory of MSB excitations coupled with optical phonons

We start by briefly reviewing the microscopic theory of MSB excitations coupled with LO phonons. For further details, we refer the reader to [28]. The total Hamiltonian of the system is given by

$$\hat{\mathrm{H}} = \hat{\mathrm{H}}_{\mathrm{e}} + \hat{\mathrm{H}}_{\mathrm{phn}} + \hat{\mathrm{H}}_{\mathrm{e\text{–}e}} + \hat{\mathrm{H}}_{\mathrm{e\text{–}phn}}, \tag{1}$$

where $\hat{\mathrm{H}}_{\mathrm{e}}$ is the bare electron Hamiltonian, $\hat{\mathrm{H}}_{\mathrm{phn}}$ is the bare phonon Hamiltonian, $\hat{\mathrm{H}}_{\mathrm{e\text{–}e}}$ is the electron–electron interaction Hamiltonian, and $\hat{\mathrm{H}}_{\mathrm{e\text{–}phn}}$ represents the electron-phonon coupling.

We start with the Hamiltonian for a single electron, $\hat{\mathrm{H}}_{\mathrm{e}} = \sum_{i\mathbf{k}} \hbar\omega_{i\mathbf{k}} \hat{\mathrm{e}}^{\dagger}_{i\mathbf{k}} \hat{\mathrm{e}}_{i\mathbf{k}}$, where $\hat{\mathrm{e}}^{\dagger}_{i\mathbf{k}}$ and $\hat{\mathrm{e}}_{i\mathbf{k}}$ are the fermionic creation and annihilation operators for an electron in subband i. The summation runs over the electronic subbands i and the in-plane momentum $\mathbf{k} \equiv (k_x, k_y)$. The subband energies are given by $\hbar\omega_{i,\mathbf{k}} = \left(\hbar^2\mathbf{k}^2\right)/(2m^*)$, where m^* is the effective electron mass accounting for the band structure of the material.

The corresponding electronic wavefunctions are given by $\Psi_i(\boldsymbol{\rho}, z) = \psi_i(z)\mathrm{e}^{\mathrm{i}\mathbf{k}\cdot\boldsymbol{\rho}}/\sqrt{S}$, where $\boldsymbol{\rho} \equiv (x, y)$, $\mathbf{k} \equiv (k_x, k_y)$, and S is the surface area of the quantum well. The function $\psi_i(z)$ describes the quantization along the growth direction and is obtained as a solution to the one-dimensional Schrödinger equation, which can be solved numerically for realistic potentials. For simplicity, we assume symmetric, square, and infinitely deep quantum wells. Under this approximation, analytical expressions for $\psi_j(z)$ and ω_j are given by [29]:

$$\psi_j(z) = \sqrt{\frac{2}{L_{\mathrm{QW}}}} \sin\left(\frac{j\pi z}{L_{\mathrm{QW}}}\right), \tag{2}$$

$$\hbar\omega_j = \frac{\hbar^2\pi^2 j^2}{2m^* L_{\mathrm{QW}}^2}, \tag{3}$$

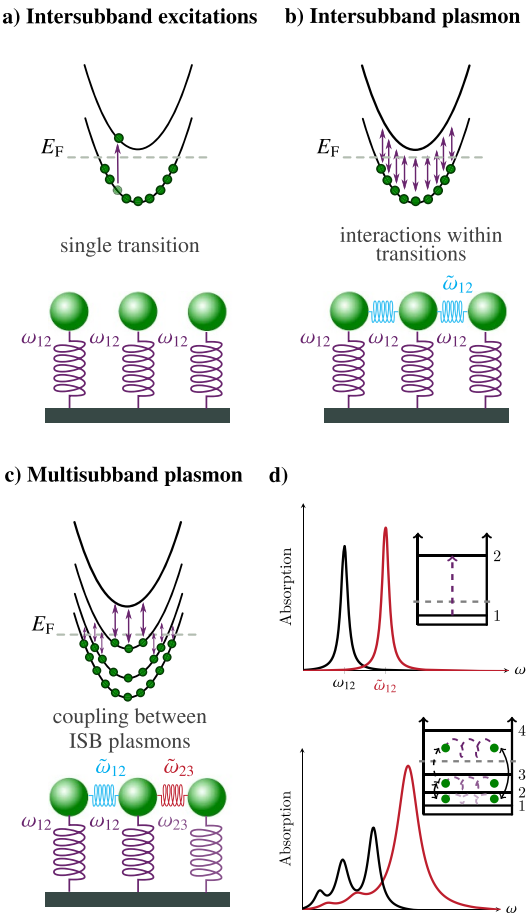

Figure 1. Physical picture of the intersubband excitations as oscillators oriented in the direction of growth of a quantum well. (a) One-particle excitation between two subbands with energy $\omega_{12,\mathbf{q}}$ where we consider only vertical transitions $\mathbf{q} = \mathbf{0}$. (b) The Coulomb interaction between the transitions (blue springs) gives rise to a collective response of the electrons, the so-called intersubband (ISB) plasmons with $\tilde{\omega}_{12}$. (c) For more than two occupied subbands, we should also consider the interactions between the different ISB plasmons are represented by springs of different colors, $\tilde{\omega}_{12}$ and $\tilde{\omega}_{23}$. These will give rise to MSB plasmons. (d) Schematized absorption spectrum of a quantum well with one occupied subband, on top, with (red) and without (black) Coulomb effects. On the bottom, the schematized spectrum considers several occupied bands. The single-particle picture (black) displays resonances at the energies of the optically active ISB transitions. Considering the dipole–dipole interactions, the coupling between ISB transitions results in MSB plasmon resonances at different energies with respect to the bare ISB transitions (red). We propose to scatter an MSB plasmon into another MSB plasmon with lower energy by emitting an LO phonon.

with population at $T = 0$ K given by

$$n_j = \frac{m^* L_{\mathrm{QW}}^2}{\pi \hbar} \left(E_{\mathrm{F}} - E_j\right),$$

where L_{QW} is the well width and E_{F} is the Fermi energy. A state is considered unoccupied if $E_j > E_{\mathrm{F}}$. While we model the quantum wells as infinite for analytical simplicity, we note that realistic finite wells would exhibit slightly lower subband energies and nonuniform spacing. This would shift the plasmon–phonon resonance conditions and slightly reduce scattering rates due to wavefunction penetration into the barriers. Nevertheless, the fundamental mechanism of phonon-mediated plasmon–plasmon scattering and the density-tunable resonances are expected to remain robust, with only quantitative adjustments required for specific material systems.

As an example, we consider a GaInAs infinite quantum well of size 200 Å with $m^* = 0.0427\ m_{\mathrm{e}}$ (with m_{e} denoting the electron rest mass), for which we find $\hbar\omega_1 = 21.8$ meV, $\hbar\omega_2 = 87.4$ meV, and $\hbar\omega_3 = 196.6$ meV. An illustration of the wavefunctions defined by equation (3), confined inside the well and vanishing outside, is shown in figure 2(a). In the following, we set the Fermi energy such that only the first and second subbands are occupied.

To describe the ISB transitions in the system, we begin by replacing the electronic Hamiltonian $\hat{\mathrm{H}}_{\mathrm{e}}$ with an effective bosonic Hamiltonian that captures excitations between subbands. These excitations correspond to the promotion of an electron from an occupied state below the Fermi level to an unoccupied

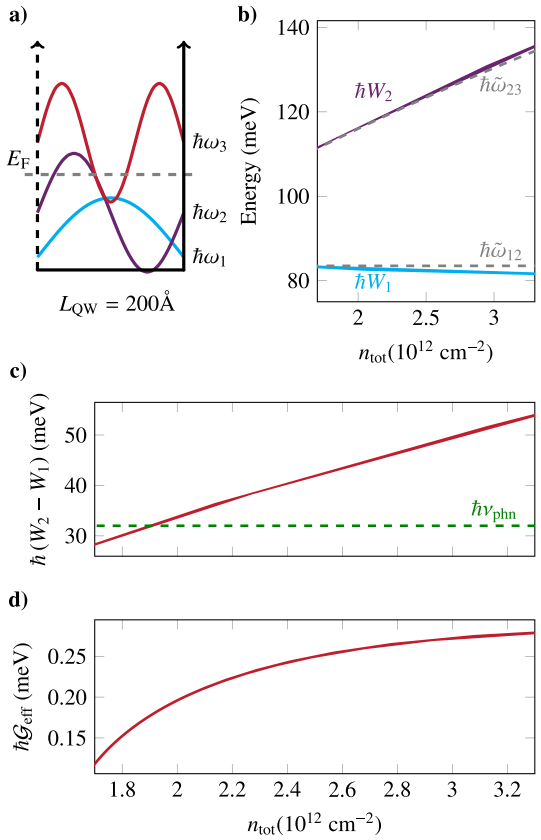

Figure 2. (a) Wavefuntions and energy levels $\omega_1 = 21.8$ meV, $\omega_2 = 87.4$ meV, and $\omega_3 = 196.6$ meV of a 200 Å an GaInAs infinite quantum well. (b) Bare intersubband energies without interactions, $\tilde{\omega}_{12}$ and $\tilde{\omega}_{23}$ (in dashed gray), and coupled MSB eigenmodes $W_{1,2}$ (in blue and purple) as a function of the total doping density n_{tot}. (c) Comparison between the $\nu_{phn} = 32$ meV energy and the difference between MSB frequencies as a function of the total doping density. The resonance condition $W_1 + \nu_{phn} = W_2$ happens at $n_{tot} \sim 1.9 \times 10^{12}\,\mathrm{cm}^{-2}$. (d) Effective coupling strength $\mathcal{G}_{eff}$ as a function of the total doping density.

state in a higher subband. For an excitation characterized by a wavevector transfer $\mathbf{q}$ — where an electron initially in state $\mathbf{k}$ is excited to state $\mathbf{k}+\mathbf{q}$ in a higher subband.

In the long-wavelength limit ($\mathbf{q} \to 0$), the excitation momentum is small compared to the typical electronic momenta, allowing us to approximate the transitions as vertical. Thus, the energy difference becomes $\mathbf{q} = 0$, $\omega_{j\mathbf{k}+\mathbf{q}} - \omega_{i\mathbf{k}} \overset{\mathbf{q}\to 0}{\approx} \omega_j - \omega_i \equiv \omega_{ji}$ [30]. Denoting the transition $\alpha \equiv i \to j$, we introduce bosonic operators $\hat{\mathrm{b}}^\dagger_{\alpha\mathbf{q}}$ and $\hat{\mathrm{b}}_{\alpha\mathbf{q}}$ to describe these ISB excitations, valid in the weak excitation limit [15]. The resulting bosonic Hamiltonian reads

$$\hat{\mathrm{H}}_\mathrm{e} = \sum_{\alpha\mathbf{q}} \hbar\omega_\alpha \hat{\mathrm{b}}^\dagger_{\alpha\mathbf{q}} \hat{\mathrm{b}}_{\alpha\mathbf{q}}, \tag{4}$$

where the bosonic operators are defined as

$$\hat{\mathrm{b}}^\dagger_{\alpha\mathbf{q}} = \frac{1}{\sqrt{\Delta n_\alpha}} \sum_{\mathbf{k}} \hat{\mathrm{e}}^\dagger_{j,\mathbf{k}+\mathbf{q}} \hat{\mathrm{e}}_{i,\mathbf{k}}, \tag{5}$$

with $\left[\hat{\mathrm{b}}_{\alpha\mathbf{q}}, \hat{\mathrm{b}}^\dagger_{\alpha\mathbf{q}}\right] = \delta_{\mathbf{q},\mathbf{q}'}$ and $\Delta n_\alpha = \langle \hat{n}_j \rangle - \langle \hat{n}_i \rangle$ representing the subband population difference.

Inclusion of electron–electron interactions introduces a collective nature to these excitations, forming ISB plasmons. The Coulomb interaction is described by [31]

$$\hat{\mathrm{H}}_{\mathrm{e\text{–}e}} = \frac{1}{2} \sum_{i,j,m,n} \sum_{\mathbf{q},\mathbf{k},\mathbf{k}'} V_{imnj,\mathbf{q}} \hat{\mathrm{e}}^\dagger_{i\mathbf{k}+\mathbf{q}} \hat{\mathrm{e}}^\dagger_{m\mathbf{k}'-\mathbf{q}} \hat{\mathrm{e}}_{n\mathbf{k}'} \hat{\mathrm{e}}_{j\mathbf{k}}, \tag{6}$$

where the factor $1/2$ accounts for the double count of the particles, and with the 2D Coulomb matrix elements given by

$$V_{imnj,\mathbf{q}} = \frac{1}{S} \frac{e^2}{2\varepsilon_0 \varepsilon_\infty |\mathbf{q}|} I_{imnj}(q), \tag{7}$$

We use the high-frequency dielectric constant ε_∞, as ε_s includes the effect of the coupling to LO phonons, which are treated exactly in our study. $I_{imnj}(q)$ accounts for the overlap of charge distributions in the quantum well:

$$I_{imnj}(q)=\int_0^L \mathrm{d}z\int_0^L \mathrm{d}z'\psi_i(z)\,\psi_j(z)\,\mathrm{e}^{-q|z-z'|}\psi_m(z')\,\psi_n(z')\,. \tag{8}$$

Using the formalism of [31–33], the combined electron and Coulomb interaction Hamiltonian can be recast in terms of bosonic ISB operators

$$\hat{\mathrm{H}}_\mathrm{e}+\hat{\mathrm{H}}_\mathrm{e\text{–}e}=\sum_{\alpha,\mathbf{q}}\hbar\omega_\alpha\hat{\mathrm{b}}^\dagger_{\alpha,\mathbf{q}}\hat{\mathrm{b}}_{\alpha,\mathbf{q}}+\sum_{\alpha,\beta,\mathbf{q}}\frac{e^2\sqrt{\Delta n_\alpha\Delta n_\beta}}{4\varepsilon_0\varepsilon_\infty S}\frac{I_{imnj}(q)}{|\mathbf{q}|}\left(\hat{\mathrm{b}}^\dagger_{\alpha,\mathbf{q}}+\hat{\mathrm{b}}_{\alpha,-\mathbf{q}}\right)\left(\hat{\mathrm{b}}^\dagger_{\beta,-\mathbf{q}}+\hat{\mathrm{b}}_{\beta,\mathbf{q}}\right). \tag{9}$$

This quadratic Hamiltonian is diagonalized via a Bogoliubov transformation, $\left[\hat{\mathrm{p}}_{\alpha,\mathbf{q}},\hat{\mathrm{H}}_\mathrm{e}+\hat{\mathrm{H}}_\mathrm{e\text{–}e}\right]=\hbar\tilde{\omega}_{\alpha,\mathbf{q}}\hat{\mathrm{p}}_{\alpha,\mathbf{q}}$, yielding new bosonic operators $\hat{\mathrm{p}}_{\alpha,\mathbf{q}}$ that describe ISB plasmons [30]

$$\hat{\mathrm{p}}_{\alpha,\mathbf{q}}=\frac{\tilde{\omega}_{\alpha,\mathbf{q}}+\omega_\alpha}{2\sqrt{\tilde{\omega}_{\alpha,\mathbf{q}}\omega_\alpha}}\hat{\mathrm{b}}_{\alpha,\mathbf{q}}+\frac{\tilde{\omega}_{\alpha,\mathbf{q}}-\omega_\alpha}{2\sqrt{\tilde{\omega}_{\alpha,\mathbf{q}}\omega_\alpha}}\hat{\mathrm{b}}^\dagger_{\alpha,\mathbf{q}}, \tag{10}$$

with eigenfrequencies

$$\tilde{\omega}_{\alpha,\mathbf{q}}=\sqrt{\omega_\alpha^2+\Theta^2_{\alpha,\mathbf{q}}}, \tag{11}$$

and the interaction-induced shift

$$\Theta^2_{\alpha,\mathbf{q}}=\frac{e^2\omega_\alpha}{\hbar\varepsilon_0\varepsilon_\infty}\frac{\Delta n_\alpha}{S}\frac{I_{\alpha\alpha}(q)}{|\mathbf{q}|}. \tag{12}$$

Note that $\Theta_{\alpha,-\mathbf{q}}=\Theta_{\alpha,\mathbf{q}}$. In the $\mathbf{q}\to 0$ limit, these correspond to the well-known *intersubband plasmon* of a 2D electron gas. The Coulomb density-density interaction generates both energy-conserving terms of the form $b^\dagger_\alpha b_\beta$ and counter-rotating terms $b_\alpha b_\beta$ and $b^\dagger_\alpha b^\dagger_\beta$. These terms are retained in the bosonized Hamiltonian and are included in the Bogoliubov transformation that yields the collective plasmon modes. The counter-rotating contributions are essential to reproduce the depolarization shift and the correct collective plasmon dispersion.

To account for the mutual coupling between distinct ISB plasmons ($\alpha\neq\beta$), we extend the Hamiltonian to an MSB basis [34]

$$\hat{\mathrm{H}}_\mathrm{e}+\hat{\mathrm{H}}_\mathrm{e\text{–}e}=\sum_{\alpha,\mathbf{q}}\hbar\tilde{\omega}_{\alpha,\mathbf{q}}\hat{\mathrm{p}}^\dagger_{\alpha,\mathbf{q}}\hat{\mathrm{p}}_{\alpha,\mathbf{q}}+\hbar\sum_{\alpha\neq\beta,\mathbf{q}}\Xi_{\alpha,\beta,\mathbf{q}}\left(\hat{\mathrm{p}}^\dagger_{\alpha,\mathbf{q}}+\hat{\mathrm{p}}_{\alpha,-\mathbf{q}}\right)\left(\hat{\mathrm{p}}^\dagger_{\beta,-\mathbf{q}}+\hat{\mathrm{p}}_{\beta,\mathbf{q}}\right) \tag{13}$$

with coupling terms

$$\Xi_{\alpha,\beta,\mathbf{q}}=\frac{\Theta_{\alpha,\mathbf{q}}\Theta_{\beta,\mathbf{q}}}{4\sqrt{\tilde{\omega}_{\alpha,\mathbf{q}}\tilde{\omega}_{\beta,\mathbf{q}}}}\frac{\mathcal{F}_{\alpha\beta}(q)}{\sqrt{\mathcal{F}_{\alpha\alpha}(q)\,\mathcal{F}_{\beta\beta}(q)}}, \tag{14}$$

and $\mathcal{F}_{\alpha\beta}(q)=I_{\alpha\beta}(q)/|\mathbf{q}|$. [Note that our study is restricted to interactions between modes where $\mathbf{q}\to 0$, as we are only concerned with the interactions between the ISB plasmons.]

The MSB plasmon Hamiltonian is then diagonalized by introducing new collective modes

$$\hat{\mathrm{P}}_{n,\mathbf{q}}=\sum_\alpha\left(x_{n\alpha}\hat{\mathrm{p}}_{\alpha,\mathbf{q}}+y_{n\alpha}\hat{\mathrm{p}}^\dagger_{\alpha,-\mathbf{q}}\right), \tag{15}$$

such that

$$\hat{\mathrm{H}}_\mathrm{MSB}=\sum_{n,\mathbf{q}}\hbar W_{n,\mathbf{q}}\hat{\mathrm{P}}^\dagger_{n,\mathbf{q}}\hat{\mathrm{P}}_{n,\mathbf{q}}. \tag{16}$$

The coefficients $\mathbf{V}_{n,\mathbf{q}}=(x_{n1},y_{n1},\ldots,x_{nN},y_{nN})^T$ are obtained by solving the corresponding Hopfield eigenproblem, $\mathbf{M}\mathbf{V}_{n,\mathbf{q}}=W_{n,\mathbf{q}}\mathbf{V}_{n,\mathbf{q}}$,

$$\left[\hat{\mathrm{p}}_{\alpha,\mathbf{q}},\hat{\mathrm{H}}_\mathrm{MSB}\right]=\hbar\tilde{\omega}_{\alpha,\mathbf{q}}\hat{\mathrm{p}}_{\alpha,\mathbf{q}}+\sum_{\alpha\neq\beta,\mathbf{q}}\hbar\Xi_{\alpha\beta,\mathbf{q}}\left(\hat{\mathrm{p}}^\dagger_{\beta,\mathbf{q}}+\hat{\mathrm{p}}_{\beta,\mathbf{q}}\right) \tag{17}$$

ensuring bosonic commutation relations via $\sum_i (|x_{ni}|^2 - |y_{ni}|^2) = 1$ [30, 35].

In figure 2(b), we compare the results for the uncoupled ISB plasmons, $\hbar\tilde{\omega}_{12,23}$, to the MSB $\hbar W_{1,2}$ arising from the collective interaction. We have done so varying the total electronic density per unit surface Δn_{tot}. The quantum well used for this example is the same as described above, where we consider the limit $\mathbf{q} \to 0$.

We now turn to the phonon realm. The free phonon Hamiltonian is expressed using 3D bosonic operators $\hat{\text{h}}^\dagger_{\mathbf{q},q_z}, \hat{\text{h}}_{\mathbf{q},q_z}$

$$\hat{\text{H}}_{\text{phn}} = \sum_{\mathbf{q},q_z} \hbar\nu_{\text{phn}} \hat{\text{h}}^\dagger_{\mathbf{q},q_z} \hat{\text{h}}_{\mathbf{q},q_z}, \tag{18}$$

assuming dispersionless optical phonons [11] — one can ignore the phonon dispersion as we are looking only at phonons with small in-plane wave vectors $\mathbf{q}$ as our study focuses on the coupling with coherent ISB excitations. Furthermore, ISB scattering is neglected, as it occurs on much faster timescales than ISB transitions [36].

The electron-phonon interaction in terms of ISB bosons becomes [11, 37]

$$\hat{\text{H}}_{\text{phn–e}} = \sum_{\alpha,\mathbf{q}} \hbar \sqrt{\frac{\nu_{\text{phn}} e^2 \Delta n_\alpha}{4\hbar\varepsilon_0\varepsilon_\rho} \frac{\omega_\alpha}{\tilde{\omega}_{\alpha,\mathbf{q}}} \frac{I_{\alpha\alpha}(q)}{|\mathbf{q}|}} \left(\hat{\text{b}}^\dagger_{\alpha,\mathbf{q}} + \hat{\text{b}}_{\alpha,-\mathbf{q}}\right) \left(\hat{\text{r}}^\dagger_{-\mathbf{q}} + \hat{\text{r}}_{\mathbf{q}}\right), \tag{19}$$

where $\varepsilon_\rho^{-1} = \varepsilon_\infty^{-1} - \varepsilon_s^{-1}$ and $\hat{\text{r}}_{\mathbf{q}}$ correspond to linear superpositions of phonon modes as the electronic transitions $\alpha : i \to j$ couple to multiple phonon modes indexed by q_z [11]. In our formalism, we describe intersubband light-matter coupling in the dipole gauge [28] and electron-LO-phonon interactions via the Fröhlich Hamiltonian, whose longitudinal nature ensures gauge consistency and avoids double-counting while correctly capturing collective and polaronic effects in MSB plasmon systems [11, 28].

Expressing the coupling in terms of MSB plasmon operators yields

$$\hat{\text{H}}_{\text{MSB-phn}} = \sum_{n,\mathbf{q}} \hbar \mathcal{G}_{n,\mathbf{q}} \left(\hat{\text{P}}^\dagger_{n,\mathbf{q}} + \hat{\text{P}}_{n,-\mathbf{q}}\right) \left(\hat{\text{r}}^\dagger_{-\mathbf{q}} + \hat{\text{r}}_{\mathbf{q}}\right), \tag{20}$$

with the coupling strength

$$\mathcal{G}_{n,\mathbf{q}} = \sum_\alpha \sqrt{\frac{\nu_{\text{phn}} e^2 \Delta n_\alpha}{4\hbar\varepsilon_0\varepsilon_\rho} \frac{\omega_\alpha}{\tilde{\omega}_\alpha} \frac{I_\alpha(q)}{|\mathbf{q}|}} X_{\alpha n}, \tag{21}$$

where $X_{\alpha n} = (x_{n\alpha} + y_{n\alpha})^{-1}$.

In summary, this formalism develops a microscopic, bosonized model of ISB excitations and their coupling to LO phonons. The resulting Hamiltonian forms the basis for analyzing light-matter interactions in quantum well systems within the electric dipole gauge for $\mathbf{q} \to 0$ [30]. For analytical insight, we continue with the simplified case of an infinite potential well of width L_{QW}, which clearly reveals the role of effective mass and phonon frequency in shaping MSB plasmon dynamics. This framework, however, can be extended to realistic confining potentials.

3. Derivation of the effective Hamiltonian

In this section, we derive a quantum-mechanical description of the effective second-order interaction between LO phonons and MSB plasmons.

We consider a transition process starting from an initial state

$$\left|\Psi_2(\mathbf{k}_2), \mathbf{0}_\mathbf{q}\right\rangle = |\mathbf{k}_2\rangle \otimes \left|\mathbf{0}_\mathbf{q}\right\rangle, \tag{22}$$

where $|\mathbf{k}_2\rangle$ denotes a MSB plasmon with wavevector $\mathbf{k}_2$ and energy W_2, and $\left|\mathbf{0}_\mathbf{q}\right\rangle$ is the phonon vacuum corresponding to in-plane momentum $\mathbf{q}$.

The system evolves to a final state

$$\left|\Psi_1(\mathbf{k}_1), \mathbf{1}_\mathbf{q}\right\rangle = |\mathbf{k}_1\rangle \otimes \left|\mathbf{1}_\mathbf{q}\right\rangle, \tag{23}$$

where $|\mathbf{k}_1\rangle$ is a lower-energy MSB plasmon state with energy W_1, and $\left|\mathbf{1}_\mathbf{q}\right\rangle$ denotes a one-phonon state with in-plane wavevector $\mathbf{q}$.

This process corresponds to the emission of a phonon by an excited MSB plasmon and occurs under the resonance condition

$$W_2 - W_1 = \nu_{\text{phn}}, \tag{24}$$

i.e. the energy difference between the initial and final MSB states matches the phonon energy.

We now consider the total Hamiltonian

$$\hat{\text{H}} = \hat{\text{H}}_{\text{MSB}} + \hat{\text{H}}_{\text{phn}} + \hat{\text{H}}_{\text{MSB-phn}}$$

which describes the interaction between optical phonons and MSB plasmons, restricted here to two MSB branches. The free MSB plasmon Hamiltonian is given by

$$\hat{\text{H}}_{\text{MSB}} = \hbar \sum_{\mathbf{q}} \sum_{\lambda=1,2} W_{\lambda,\mathbf{q}} \hat{\text{P}}^{\dagger}_{\lambda,\mathbf{q}} \hat{\text{P}}_{\lambda,\mathbf{q}}, \tag{25}$$

while the MSB plasmon–phonon interaction Hamiltonian reads

$$\hat{\text{H}}_{\text{MSB-phn}} = \sum_{\lambda=1,2} \sum_{\mathbf{q}} \hbar\, \mathcal{G}_{\lambda,\mathbf{q}} \left(\hat{\text{P}}^{\dagger}_{\lambda,\mathbf{q}} + \hat{\text{P}}_{\lambda,-\mathbf{q}} \right) \left(\hat{\text{r}}^{\dagger}_{-\mathbf{q}} + \hat{\text{r}}_{\mathbf{q}} \right). \tag{26}$$

The equations of motion for the MSB and phonon mode operators are obtained using Heisenberg's equation of motion, $i\hbar\dot{\hat{O}} = \left[\hat{O}, \hat{\text{H}}\right]$ applied to the relevant bosonic operators. For the MSB plasmon operators, we find

$$\dot{\hat{\text{P}}}_{n,\mathbf{q}}(t) = \frac{\text{i}}{\hbar} \left[\hat{\text{H}}, \hat{\text{P}}_{n,\mathbf{q}}\right] = -\text{i} W_{n,\mathbf{q}} \hat{\text{P}}_{n,\mathbf{q}}(t) - \text{i}\mathcal{G}_{n,\mathbf{q}} \left(\hat{\text{r}}^{\dagger}_{-\mathbf{q}}(t) + \hat{\text{r}}_{\mathbf{q}}(t) \right), \tag{27}$$

and the phononic mode operator

$$\dot{\hat{\text{r}}}_{\mathbf{k}}(t) = \frac{\text{i}}{\hbar} \left[\hat{\text{H}}, \hat{\text{r}}_{\mathbf{k}}\right] = -\text{i}\nu_{\text{phn}} \hat{\text{r}}_{\mathbf{k}}(t) - \text{i} \sum_{\lambda} \mathcal{G}_{\lambda,\mathbf{k}} \left(\hat{\text{P}}^{\dagger}_{\lambda,\mathbf{k}}(t) + \hat{\text{P}}_{\lambda,-\mathbf{k}}(t) \right). \tag{28}$$

These equations are the basis of everything that follows from now on. These are coupled differential operator equations and not solvable in closed form. We attempt to solve equation (28) by formally integrating it

$$\hat{\text{r}}_{\mathbf{k}}(t) = \text{e}^{-\text{i}\nu_{\text{phn}} t} \hat{\text{r}}_{\mathbf{k}}(0) - \text{i} \sum_{\lambda} \mathcal{G}_{\lambda,\mathbf{k}} \int_0^t \text{d}t' \text{e}^{-\text{i}\nu_{\text{phn}}(t-t')} \left(\hat{\text{P}}^{\dagger}_{\lambda,\mathbf{k}}(t') + \hat{\text{P}}_{\lambda,-\mathbf{k}}(t)' \right). \tag{29}$$

The first term in equation (29) is the free evolution of the phononic mode operator, whereas the second term describes the influence of the interaction. The temporal integral is, of course, tricky since we do not know the temporal evolution of the ISB operators. Nevertheless, we can approximate the integral using the rotating-wave approximation in which we assume that the ISB consists of a slowly varying part and a rapidly oscillating contribution that evolves with W_λ,

$$\hat{\text{P}}_{\lambda,-\mathbf{k}}(t') = \hat{\tilde{P}}_{\lambda,-\mathbf{k}}(t') \text{e}^{-\text{i}W_{\lambda,\mathbf{k}} t'},$$
$$\hat{\text{P}}^{\dagger}_{\lambda,\mathbf{k}}(t') = \hat{\tilde{P}}^{\dagger}_{\lambda,\mathbf{k}}(t') \text{e}^{\text{i}W_{\lambda,\mathbf{k}} t'}.$$

Then we take the slow envelope $\hat{\tilde{p}}_\alpha$ out of the integral at the upper time t and replace it with its full operator function,

$$\begin{aligned} &\int_0^t \text{d}t' \text{e}^{-\text{i}\nu_{\text{phn}}(t-t')} \left(\hat{\text{P}}^{\dagger}_{\lambda,\mathbf{k}}(t') + \hat{\text{P}}_{\lambda,-\mathbf{k}}(t') \right) \\ &\quad = \hat{\text{P}}^{\dagger}_{\lambda,\mathbf{k}}(t) \int_0^t \text{d}t' \text{e}^{-\text{i}\left(W_{\lambda,\mathbf{k}} + \nu_{\text{phn}}\right)(t-t')} + \hat{\text{P}}_{\lambda,-\mathbf{k}}(t) \int_0^t \text{d}t' \text{e}^{\text{i}\left(W_{\lambda,\mathbf{k}} - \nu_{\text{phn}}\right)(t-t')}. \end{aligned} \tag{30}$$

This approximation is also called the Markov approximation, in which information from past times has been erased. To justify the use of the Markov approximation, we compare the relevant timescales of the system. The phonon correlation time is given by $\tau_{\text{ph}} \sim 1/\Gamma_{\text{phn}}$. For GaInAs quantum wells, $\hbar\Gamma_{\text{phn}} \sim 1.5$ meV, corresponding to $\tau_{\text{ph}} \sim 0.5$ ps. The effective plasmon–plasmon scattering rate mediated by phonons is $G_{\text{eff}} \sim 0.2$ meV for the carrier densities considered, yielding a timescale $1/G_{\text{eff}} \sim 3.3$ ps. Since

$\tau_{\rm ph} \lesssim 1/G_{\rm eff}$, the phonon bath relaxes on a timescale shorter than or comparable to that of the plasmon dynamics, thereby validating a Markovian treatment. This indicates that, despite the resonant nature of the interaction, memory effects are weak, and the scattering rates are well captured by the present approach.

The integrals can be approximated in the long-time limit, i.e. by extending the upper limit of integration to infinity,

$$\int_0^t \mathrm{d}t' \mathrm{e}^{\mathrm{i}\left(\nu_{\rm phn}+W_{\lambda,\mathbf{k}}\right)\left(t-t'\right)} \approx -\frac{1}{\mathrm{i}\left(\nu_{\rm phn}+W_{\lambda,\mathbf{k}}\right)}.$$

such that,

$$\hat{\mathrm{r}}_{\mathbf{k}}\left(t\right) = \mathrm{e}^{-\mathrm{i}\nu_{\rm phn}t}\hat{\mathrm{r}}_{\mathbf{k}}\left(0\right) - \sum_{\lambda}\mathcal{G}_{\lambda,\mathbf{k}}\left(\hat{\mathrm{P}}^{\dagger}_{\lambda,\mathbf{k}}\left(t\right)\frac{1}{\left(W_{\lambda,\mathbf{k}}+\nu_{\rm phn}\right)} - \hat{\mathrm{P}}_{\lambda,-\mathbf{k}}\left(t\right)\frac{1}{\left(W_{\lambda,\mathbf{k}}-\nu_{\rm phn}\right)}\right). \tag{31}$$

Replacing in the MSB plasmon equation of motion

$$\dot{\hat{\mathrm{P}}}_{n,-\mathbf{q}}\left(t\right) = -\mathrm{i}W_{n,\mathbf{q}}\hat{\mathrm{P}}_{n,-\mathbf{q}}\left(t\right) - \mathrm{i}\mathcal{G}_{n,\mathbf{q}}\sum_{\lambda}\mathcal{G}_{\lambda,\mathbf{q}}\left(\frac{\hat{\mathrm{P}}^{\dagger}_{\lambda,\mathbf{q}}\left(t\right)}{\left(W_{\lambda,\mathbf{q}}-\nu_{\rm phn}\right)} - \frac{\hat{\mathrm{P}}_{\lambda,-\mathbf{q}}\left(t\right)}{\left(W_{\lambda,\mathbf{q}}+\nu_{\rm phn}\right)}\right)$$
$$+\mathrm{i}\mathcal{G}_{n,\mathbf{q}}\sum_{\lambda}\mathcal{G}_{\lambda,-\mathbf{q}}\left(\frac{\hat{\mathrm{P}}^{\dagger}_{\lambda,\mathbf{q}}\left(t\right)}{\left(W_{\lambda,\mathbf{q}}+\nu_{\rm phn}\right)} - \frac{\hat{\mathrm{P}}_{\lambda,-\mathbf{q}}\left(t\right)}{\left(W_{\lambda,\mathbf{q}}-\nu_{\rm phn}\right)}\right).$$

Recalling the resonance condition $W_2 - \nu_{\rm phn} = W_1$, we apply the rotating wave approximation and finally arrive at the effective equation of motion describing the dynamics of the resonant phonon-MSB plasmon coupling, where

$$\dot{\hat{\mathrm{P}}}_{1,-\mathbf{q}}\left(t\right) = -\mathrm{i}W_{1,\mathbf{q}}\hat{\mathrm{P}}_{1,-\mathbf{q}}\left(t\right) + \mathrm{i}\mathcal{G}_{1,\mathbf{q}}\left(\frac{\mathcal{G}_{2,\mathbf{q}}}{W_{2,\mathbf{q}}+\nu_{\rm phn}} - \frac{\mathcal{G}_{2,-\mathbf{q}}}{W_{2,\mathbf{q}}-\nu_{\rm phn}}\right)\hat{\mathrm{P}}_{2,-\mathbf{q}}\left(t\right). \tag{32}$$

The equations of motion derived above can be interpreted as arising from an effective second-order interaction Hamiltonian of the form

$$\hat{\mathrm{H}}_{\rm int(eff)} = -\hbar\sum_{\mathbf{q}}\mathcal{G}_{1,\mathbf{q}}\mathcal{G}_{2,\mathbf{q}}\frac{2\nu_{\rm phn}}{\nu_{\rm phn}^2 - W_{2,\mathbf{q}}^2}\hat{\mathrm{P}}^{\dagger}_{1,\mathbf{q}}\hat{\mathrm{P}}_{2,-\mathbf{q}}. \tag{33}$$

which describes a phonon-mediated process in which one MSB plasmon is annihilated while another is created. The bosonic quantization of MSB plasmons employed here is formally exact only in the linear (low-excitation) regime, where the number of excited plasmons is much smaller than the total carrier population [15, 38]. Within the random-phase approximation (RPA), the collective MSB plasmon operators P_ν emerge from the diagonalization of the electronic density-density Hamiltonian and satisfy approximately bosonic commutation relations,

$$\left[P_\nu, P^{\dagger}_{\nu'}\right] = \delta_{\nu,\nu'} + \mathcal{O}\left(N_{\rm exc}/N_{\rm e}\right).$$

The nonlinear decay process considered in this work—where one high-energy plasmon scatters into a lower-energy plasmon via longitudinal-optical phonon emission—lies well within the few-excitation limit, such that deviations from ideal bosonic behavior (phase-space filling or saturation) are negligible. For the nonlinear scattering process studied, the bosonic approximation is valid only if the plasmon occupation remains much smaller than the number of electrons in the subbands. At higher densities, higher-order corrections cannot be ignored and will modify both decay rates and the plasmon statistics; these nonbosonic corrections would manifest as anharmonic renormalizations of the plasmon–plasmon and plasmon–phonon couplings, which could be captured through a Holstein-Primakoff expansion or beyond-RPA treatments, but such effects are outside the excitation regime relevant here.

To illustrate this effect, we consider a GaInAs quantum well with an infinite potential profile and two occupied subbands. The relevant ISB transitions are $1 \to 2$ and $2 \to 3$, which give rise to two collective MSB plasmon branches (see figure 2(b)). As shown in figure 2(c), we compare the LO phonon energy, $\hbar\nu_{\rm phn} = 32$ meV, with the energy difference between the two MSB modes as a function of doping. A resonant condition is achieved when $\hbar W_1 = 82.8$ meV (lower MSB branch) and $\hbar W_2 = 114.8$ meV (upper branch), such that $W_2 - W_1 = \nu_{\rm phn}$. Numerical evaluation under these conditions yields an effective second-order coupling strength of approximately 0.17 meV, an order of magnitude smaller than the

coupling strength of a single MSB plasmon and a phonon [28]. While the current analysis assumes $T = 0\,\mathrm{K}$, the model can be extended to finite temperatures by incorporating the thermal electronic population of the subbands. Note that, for MSB plasmons undergoing nonlinear scattering, we estimate the mode linewidths to be on the order of a few meV under low-temperature, moderate-doping, high-quality quantum well conditions. At elevated plasmon occupation, the linewidth is expected to increase due to enhanced scattering, transition saturation, and many-body dephasing.

Finally, we evaluate the scattering rate of an MSB plasmon induced by the emission of an optical phonon, wherein an initial MSB pump mode decays into a lower-energy signal mode. As the phonon-mediated MSB-MSB coupling lies in the weak-coupling regime, the scattering rate can be calculated using Fermi's Golden Rule.

This process corresponds to a transition from the initial state

$$|I\rangle = \hat{\mathrm{P}}^{\dagger}_{2,-\mathbf{q}}|\mathrm{GS}\rangle\,, \tag{34}$$

to the final state

$$|F\rangle = \hat{\mathrm{P}}^{\dagger}_{1,\mathbf{q}}|\mathrm{GS}\rangle\,, \tag{35}$$

where $|\mathrm{GS}\rangle$ denotes the ground state of the system. Applying Fermi's Golden Rule to the effective second-order interaction Hamiltonian $\hat{\mathrm{H}}^{(\mathrm{eff})}_{\mathrm{int}}$ yields the scattering rate

$$\Gamma_{\mathrm{scat}} = \frac{2\pi}{\hbar}\left|\langle F|\,\hat{\mathrm{H}}^{(\mathrm{eff})}_{\mathrm{int}}\,|I\rangle\right|^2 \delta\left(E_{\mathrm{F}} - E_I\right). \tag{36}$$

The application of Fermi's Golden Rule to calculate the scattering rate Γ_{scat} in equation (36) is justified despite the discrete nature of MSB plasmon states due to three key physical considerations: (i) first, the emission of LO phonons couples the plasmonic system to a continuum of phonon modes, effectively broadening the final state density. This satisfies the fundamental requirement for irreversible transitions [39]. The phonon spectral function, characterized by its linewidth Γ_{phn}, replaces the delta function with a Lorentzian density of states, as implemented below in equation (41); (ii) second, the Markov approximation inherent in our derivation of the effective Hamiltonian (section 3) ensures time-irreversibility by neglecting memory effects. This approximation is valid when the phonon bath correlation time ($\sim 1/\Gamma_{\mathrm{phn}}$) is much shorter than the plasmon dynamics timescale ($\sim 1/|\mathcal{G}_{n,\mathbf{q}}|$) [40]; (iii) finally, the resonant energy matching condition $W_2 - W_1 = \nu_{\mathrm{phn}}$ maximizes the transition matrix element while the finite phonon linewidth Γ_{phn} guarantees spectral overlap. This combination enables discrete-to-discrete transitions provided the condition $|\langle F|\hat{\mathrm{H}}^{(\mathrm{eff})}_{\mathrm{int}}|I\rangle| \gg \hbar\Gamma_{\mathrm{phn}}$, as established in cavity quantum electrodynamics frameworks for discrete systems coupled to broad reservoirs [11].

Since we are considering thermally excited MSB plasmons, the standard perturbation-theory formulation must be extended from pure states to statistical ensembles. In this context, the system is described by a thermal density matrix rather than a single state vector. The thermal density matrix at temperature T, expressed in the Fock basis $|N\rangle$, takes the form

$$\hat{\rho}_{\mathrm{th}} = \sum_N p_N |N\rangle\langle N| = \sum_N \frac{\mathrm{e}^{-N\hbar\Omega_N/k_{\mathrm{B}}T}}{Z(T)}|N\rangle\langle N|\,, \tag{37}$$

where Ω_N is the energy associated with the N-plasmon Fock state and $Z(T) = \sum_M \mathrm{e}^{-M\hbar\Omega_M/k_{\mathrm{B}}T}$ is the canonical partition function.

Up to this point, we have evaluated the interaction matrix element for a process involving the transition from a single initially excited MSB plasmon mode with frequency W_1 to a final state containing a single MSB plasmon at frequency W_2. To describe a thermally excited system, this treatment must be generalized to include initial states with arbitrary occupation numbers. Specifically, we consider a thermal ensemble where the initial state contains M plasmons at frequency W_1 and N plasmons at frequency W_2. In this case, the transition probability is obtained by averaging over the thermal distribution of initial states. The corresponding expression for the squared matrix element becomes

$$\left|\langle F|\,\hat{\mathrm{H}}_{\mathrm{int(eff)}}\,|I\rangle\right|^2 = \mathrm{Tr}\left[\hat{\mathrm{H}}_{\mathrm{int(eff)}}\hat{\rho}_{\mathrm{in}}\hat{\mathrm{H}}_{\mathrm{int(eff)}}\,|F\rangle\langle F|\right] \tag{38}$$

where $\hat{\rho}_{\mathrm{in}}$ denotes the thermal density matrix of the initial MSB plasmon ensemble.

$$\hat{\rho}_{\mathrm{in}} = \hat{\rho}_{\mathrm{th}}(W_1) \otimes \hat{\rho}_{\mathrm{th}}(W_2) = \sum_{N,M} p^{(2)}_M p^{(1)}_N |M_2, N_1\rangle\langle M_2, N_1|\,. \tag{39}$$

Due to the form of the effective interaction Hamiltonian $\hat{\mathrm{H}}_{(\mathrm{int})\mathrm{eff}} \propto \hat{\mathrm{P}}_1^{\dagger}\hat{\mathrm{P}}_2$ the only final state $|F\rangle$ that provides a non-vanishing matrix element will be $|F\rangle = |(\mathbf{M}-\mathbf{1})_2, (\mathbf{N}+\mathbf{1})_1\rangle$. Recalling that $\hat{\mathrm{P}}\,|\mathbf{K}\rangle = \sqrt{K}\,|\mathbf{K}-\mathbf{1}\rangle$ and $\hat{\mathrm{P}}^{\dagger}\,|\mathbf{K}\rangle = \sqrt{K+1}\,|\mathbf{K}+\mathbf{1}\rangle$, one finds

$$\left|\langle F|\,\hat{\mathrm{H}}_{\mathrm{int(eff)}}\,|I\rangle\right|^2 = \sum_{M,N} p_M^{(2)} p_N^{(1)}\,(M)_{(2)}\,(N+1)_{(1)}\,U_{\mathrm{int(eff)}}^2 = \bar{N}_{\mathrm{th}}\,(W_2)\,[\bar{N}_{\mathrm{th}}\,(W_1)+1]\,U_{\mathrm{int(eff)}}^2, \tag{40}$$

where $U_{\mathrm{int(eff)}}^2 = \left|\langle F|\,\hat{\mathrm{H}}_{\mathrm{int(eff)}}\,|I\rangle\right|^2$ is the interacting potential. This result is intuitively clear: the initial MSB plasmon with frequency W_2 must be thermally populated before the resonant interaction can occur. To describe the spectral function of the optical phonon, one neglects the phonon dispersion and uses a Lorentzian shape of width Γ_{phn} where its maximum value is given by $2/\left(\pi\,\Gamma_{\mathrm{phn}}\right)$. Combining the previous results, using Fermi's Golden Rule, the scattering rate at any given temperature is given by

$$\Gamma_{\mathrm{scat}} = \bar{N}_2\,[\bar{N}_1+1]\,\frac{16}{\left(\nu_{\mathrm{phn}}^2 - W_{2,\mathbf{q}}^2\right)^2}\,\frac{\nu_{\mathrm{phn}}^2}{\Gamma_{\mathrm{phn}}}\left|\mathcal{G}_{1,\mathbf{q}}\mathcal{G}_{2,\mathbf{q}}\right|^2, \tag{41}$$

where we have introduced the compact notation $\bar{N}_i \equiv \bar{N}_{\mathrm{th}}(W_i)$ and we assumed $\nu_{\mathrm{phn}}/\Gamma_{\mathrm{phn}} \approx 50$.

In our envisaged situation, for the resonant situation, at zero temperature, numerical simulations arrive at $\Gamma_{\mathrm{scat}} \sim 10\,\mathrm{ns}^{-1}$, where the resonant condition is at total electron density $n_{\mathrm{tot}} = 1.89\times10^{12}\,\mathrm{cm}^{-2}$. In [24], it has been demonstrated that the MSB plasmon resonances of a highly doped quantum well can be excited by applying a current through a source-drain contact. The MSB plasmon superradiantly decays into free space, with a rate proportional to the electronic density in the quantum well. In GaInAs quantum wells, the spontaneous emission can reach a few picoseconds, six orders of magnitude faster than for a single particle at a similar wavelength [26]. This value is much shorter than the characteristic time of any non-radiative scattering event [36]. As such, the energy relaxation dynamics of the plasmon can be dominated by the non-radiative scattering event. The rate of this scattering process is comparable to the typical loss rates for radiative processes of the MSB plasmon modes $\Gamma_{\mathrm{rad}} \sim 10\ \mathrm{ps}^{-1} \equiv \Gamma_{\mathrm{loss}}$ [26]. Before we conclude, it might be interesting to discuss the influence of finite-temperature effects, as the scattering rate in equation (41), $\Gamma_{\mathrm{scat}}(T) = \Gamma_{\mathrm{scat}}(0)\bar{N}_2(\bar{N}_1(T)+1)$, is explicitly temperature-dependent. Here, $\bar{N}_1(T) = (\mathrm{e}^{-\beta W_2}-1)^{-1}$ represents the thermal occupation of the relevant mode. For the MSB energy splittings considered in this work ($W_2 \sim 100\,\mathrm{meV}$), the thermal occupation remains negligible even at room temperature, with $\bar{N}_1(300\,\mathrm{K}) \simeq 0.021$. At cryogenic temperatures (e.g. 77 K), this value becomes vanishingly small ($\bar{N}_1 \sim 10^{-7}$). We therefore conclude that thermal effects do not significantly impact the strong coupling regime for the proposed system.

3.1. Experimental detection of phonon-mediated MSB-MSB plasmon scattering

The resonant second-order scattering channel identified in this work provides a distinct pathway for energy relaxation in MSB quantum wells. Its experimental observation requires probing both the collective MSB modes and their coupling to LO phonons [28]. Such scattering may manifest as density-dependent cross-peaks in 2D plasmon spectra or as anti-Stokes shifts in plasmon emission, with characteristic timescales comparable to radiative decay timescales. These signatures provide a direct avenue for verifying our theoretical predictions and for exploring controlled energy relaxation and decoherence in low-dimensional semiconductor systems. Several complementary approaches can be considered:

(i) IR pump–probe spectroscopy. Resonant excitation of a high-energy MSB plasmon with an IR pulse can populate the initial plasmon state. Subsequent transfer of population to a lower-energy plasmon via LO-phonon emission manifests as a temporal modulation of absorption or transmission at the lower plasmon energy. Observation of decay dynamics faster than radiative or single-particle relaxation would constitute direct evidence of the phonon-mediated process [8, 41].

(ii) Raman scattering. Inelastic light scattering provides a complementary probe of energy and momentum transfer between collective excitations. Phonon-mediated MSB-MSB plasmon scattering is expected to generate secondary Raman peaks at energies corresponding to the initial plasmon minus the LO-phonon energy plus the final plasmon. The intensity of these peaks should scale with carrier density, reflecting the predicted density-tunable resonance [42, 43].

(iii) Terahertz and IR emission. The decay of high-energy plasmons into lower-energy modes accompanied by phonon emission can produce secondary emission in the terahertz or mid-IR range. Detection of emission at energies matching the final plasmon mode, with intensity resonantly modulated by carrier density, provides an additional unambiguous signature [28].

(iv) Density-dependent resonance. The scattering process exhibits a strong dependence on the electron density, which can be tuned via gating, providing direct experimental access to phonon-mediated MSB-MSB plasmon scattering, enabling the study of nonlinear collective dynamics in low-dimensional semiconductor systems, and guiding temperatures further distinguishes this process from competing thermal relaxation channels [44].

Taken together, these approaches allow for direct experimental access to phonon-mediated MSB-MSB plasmon scattering, enabling the study of nonlinear collective dynamics in low-dimensional semiconductor systems and providing guidance for the design of quantum well devices with tailored energy-relaxation properties. Understanding this scattering mechanism provides practical guidance for the design of IR photodetectors and QCLs, where reducing unwanted plasmon–phonon scattering can enhance device efficiency and suppress decoherence. In contrast, controlled enhancement of this process may be used in plasmonic quantum devices to engineer specific energy-relaxation pathways. The density-dependent resonance conditions identified in this work provide an experimental handle via carrier density tuning or electrostatic gating, enabling dynamic control of plasmon lifetimes and scattering rates. These results further provide insight into the interplay between collective electronic excitations and lattice vibrations in low-dimensional systems, with potential implications for thermal management and coherent phenomena in engineered nanostructures.

4. Conclusion

We developed a quantum-theoretical framework for a second-order effective interaction between MSB plasmons in low-dimensional electron systems. Our work establishes the phonon-mediated decay process (high-energy MSB plasmon $\rightarrow$ low-energy MSB plasmon + LO phonon) as a critical energy relaxation pathway. Numerical simulations quantify its dependence on material parameters and reveal its magnitude relative to first-order processes in 2D electron gases.

The versatility of our approach enables extension to a broad range of material systems and doping configurations, offering significant flexibility for future device-specific optimization. As a demonstration, we applied the model to an infinite GaInAs quantum well, identifying resonant scattering rates ($\sim 10\,\mathrm{ns}^{-1}$) competitive with radiative losses. This quantitative insight enables targeted suppression (or enhancement) of this scattering channel via doping control—a critical design lever for optimizing plasmonic devices.

From a fundamental perspective, plasmon–phonon inelastic scattering serves as a key mechanism for energy relaxation and thermalization in quantum wells and related nanostructures [45–47]. MSB plasmons naturally arise in these systems, which form the basis of THz detectors, IR photodetectors, and QCLs. For IR photodetectors, suppressing this process extends plasmon lifetimes, directly enhancing photoresponsivity [4]. In QCLs, minimizing phonon-mediated plasmon decay reduces carrier heating, potentially boosting wall-plug efficiency by $\sim 10\% - 15\%$ at optimal doping densities [48]. The plasmon–phonon coupling directly influences critical device properties, including gain bandwidth via reduced plasmon lifetime, linewidth broadening via phonon-induced dephasing, and carrier relaxation times that govern device repetition rates. In particular, for systems such as QCLs, where carriers are driven into high-energy subbands, understanding this second-order scattering process provides insight into carrier-cooling pathways that ultimately limit device speed and efficiency [36]. More broadly, this mechanism plays a central role in shaping the performance of nanoscale optoelectronic and photonic devices, and may also find utility in emerging quantum technologies, where engineered dissipation enables (i) initialization of plasmonic qubits via phonon-assisted cooling [49, 50], (ii) thermal management in integrated plasmonic circuits [51, 52], and (iii) phonon-lasing by leveraging stimulated plasmon decay [53, 54]. Hopefully, our framework provides the foundation for harnessing these collective excitations in next-generation quantum engineering.

Data availability statement

The article is theoretical, no data is available. The data that support the findings of this study are available upon reasonable request from the authors.

Acknowledgments

SR would like to acknowledge financial support from the Max Planck Society.

ORCID iDs

Sofia Ribeiro 0000-0002-8234-416X
Hugo Terças 0000-0003-2826-4377

References

[1] Helm M 1999 The Basic Physics of Intersubband Transitions *Semiconductors and Semimetals* vol 62, ed H C Liu and F Capasso (Elsevier) pp 1–99
[2] Sze S M and Ng K K 2006 *Physics of Semiconductor Devices* 3rd edn (Wiley) (available at: https://doi.org/10.1002/0470068329)
[3] Ando T, Fowler A B and Stern F 1982 Electronic properties of two-dimensional systems *Rev. Mod. Phys.* **54** 437–672
[4] Schneider H and Liu H C 2014 *Quantum Well Infrared Photodetectors: Physics and Applications* 2007th edn (Springer)
[5] Kempa K, Gornik E, Unterrainer K, Kast M and Strasser G 2001 Resonant tunneling mediated by resonant emission of intersubband plasmons *Phys. Rev. Lett.* **86** 2850–3
[6] Colombelli R, Ciuti C, Chassagneux Y and Sirtori C 2005 Quantum cascade intersubband polariton light emitters *Semicond. Sci. Technol.* **20** 985
[7] Colombelli R and Manceau J M 2015 Perspectives for intersubband polariton lasers *Phys. Rev. X* **5** 011031
[8] Manceau J-M,Tran N-L, Biasiol G, Laurent T, Sagnes I, Beaudoin G, De Liberato S, Carusotto I and Colombelli R 2018 Resonant intersubband polariton-LO phonon scattering in an optically pumped polaritonic device *Appl. Phys. Lett.* **112** 191106
[9] Apostolova T, Huang D and Cardimona D A 2003 Photon-absorption-induced intersubband optical-phonon scattering of electrons in quantum wells *Phys. Rev. B* **67** 205323
[10] Haboeck U, Goñi A R, Danckwerts M, Thomsen C and Eberl K 2000 Coupling of intersubband charge-density excitations to longitudinal-optical phonons in modulation-doped GaAs quantum wells *Solid State Commun.* **115** 85–88
[11] De Liberato S and Ciuti C 2012 Quantum theory of intersubband polarons *Phys. Rev. B* **85** 125302
[12] Schneider H and Liu HC 2007 Photoconductive QWIP *Quantum Well Infrared Photodetectors: Physics and Applications* (Springer) pp 45–81 (available at: https://doi.org/10.1007/978-3-540-36324-8_4)
[13] Dini D, Köhler R, Tredicucci A, Biasiol G and Sorba L 2003 Microcavity polariton splitting of intersubband transitions *Phys. Rev. Lett.* **90** 116401
[14] Ciuti C, Bastard G and Carusotto I 2005 Quantum vacuum properties of the intersubband cavity polariton field *Phys. Rev. B* **72** 115303
[15] De Liberato S and Ciuti C 2009 Stimulated scattering and lasing of intersubband cavity polaritons *Phys. Rev. Lett.* **102** 136403
[16] Jouy P, Vasanelli A, Todorov Y, Delteil A, Biasiol G, Sorba L and Sirtori C 2011 Transition from strong to ultrastrong coupling regime in mid-infrared metal-dielectric-metal cavities *Appl. Phys. Lett.* **98** 231114
[17] Franckié M, Ndebeka-Bandou C, Ohtani K and Faist J 2018 Quantum model of gain in phonon-polariton lasers *Phys. Rev. B* **97** 075402
[18] Delteil A, Vasanelli A, Jouy P, Barate D, Moreno J C, Teissier R, Baranov A N and Sirtori C 2011 Optical phonon scattering of cavity polaritons in an electroluminescent device *Phys. Rev. B* **83** 081404
[19] Geiser M, Castellano F, Scalari G, Beck M, Nevou L and Faist J 2012 Ultrastrong coupling regime and plasmon polaritons in parabolic semiconductor quantum wells *Phys. Rev. Lett.* **108** 106402
[20] Delteil A *et al* 2012 Charge-induced coherence between intersubband plasmons in a quantum structure *Phys. Rev. Lett.* **109** 246808
[21] Pegolotti G, Vasanelli A, Todorov Y and Sirtori C 2014 Quantum model of coupled intersubband plasmons *Phys. Rev. B* **90** 035305
[22] Montes Bajo M *et al* 2018 Multisubband plasmons in Doped Zn O quantum wells *Phys. Rev. Appl.* **10** 024005
[23] Bajo M M, Chauveau J-M, Vasanelli A, Delteil A, Todorov Y, Sirtori C and Hierro A 2023 Perspectives and opportunities with multisubband plasmonics *J. Appl. Phys.* **134** 010901
[24] Huppert S, Vasanelli A, Laurent T, Todorov Y, Pegolotti G, Beaudoin G, Sagnes I and Sirtori C 2015 Radiatively broadened incandescent sources *ACS Photonics* **2** 1663–8
[25] Niu Y, Gao L, Xu H and Wei H 2023 Strong coupling of multiple plasmon modes and excitons with excitation light controlled active tuning *Nanophotonics* **12** 735–42
[26] Laurent T 2015 Superradiant emission from a collective excitation in a semiconductor *Phys. Rev. Lett.* **115** 187402
[27] Laurent T, Todorov Y, Vasanelli A, Sagnes I, Beaudoin G and Sirtori C 2015 Electrical excitation of superradiant intersubband plasmons *Appl. Phys. Lett.* **107** 241112
[28] Ribeiro S, Vasanelli A, Todorov Y and Sirtori C 2020 Quantum theory of multisubband plasmon- phonon coupling *Photonics* **7** 19
[29] Griffiths D J 1995 *Introduction to Quantum Mechanics* (Prentice Hall)
[30] Todorov Y and Sirtori C 2012 Intersubband polaritons in the electrical dipole gauge *Phys. Rev. B* **85** 045304
[31] Nikonov D E, Amc I, Butov L V and Schmidt H 1997 Collective intersubband excitations in quantum wells: Coulomb interaction versus subband dispersion *Phys. Rev. Lett.* **79** 4633–6
[32] Lee S C and Galbraith I 1999 Intersubband and intrasubband electronic scattering rates in semiconductor quantum wells *Phys. Rev. B* **59** 15796–805
[33] Lee S-C and Galbraith I 2000 Influence of exchange scattering and dynamic screening on electron-electron scattering rates in semiconductor quantum wells *Phys. Rev. B* **62** 15327–30
[34] Todorov Y, Andrews A M, Colombelli R, De Liberato S, Ciuti C, Klang P, Strasser G and Sirtori C 2010 Ultrastrong light-matter coupling regime with polariton dots *Phys. Rev. Lett.* **105** 196402
[35] Todorov Y, Tosetto L, Delteil A, Vasanelli A, Sirtori C, Andrews A M and Strasser G 2012 Polaritonic spectroscopy of intersubband transitions *Phys. Rev. B* **86** 125314
[36] Ferreira R and Bastard G 1989 Evaluation of some scattering times for electrons in unbiased and biased single- and multiple-quantum-well structures *Phys. Rev. B* **40** 1074–86
[37] Fröhlich H 1954 Electrons in lattice fields *Adv. Phys.* **3** 325–61
[38] Christiansen M R, Hainzl C and Nam P T 2022 On the effective quasi-bosonic Hamiltonian of the electron gas: collective excitations and plasmon modes *Lett. Math. Phys.* **112** 114
[39] Cohen-Tannoudji C, Diu B and Laloë F 2019 *Quantum Mechanic, Volume II* 2nd edn (Wiley)
[40] Breuer H P and Petruccione F 2007 *The Theory of Open Quantum Systems* (Oxford University PressOxford) (available at: http://dx.doi.org/10.1093/acprof:oso/9780199213900.001.0001)

[41] Aleshkin V Y and Dubinov A A 2024 Electron-optical phonon scattering in doped GaAs quantum well *Phys. Rev. Mater.* **8** 074602
[42] Wagner J, Schmitz J, Richards D, Ralston J D and Koidl P 1996 Intersubband Raman scattering in InAsAlSb quantum wells *Solid-State Electron.* **40** 281–5
[43] Silva A A P, Vasconcellos A R and Luzzi R 2006 Resonant Raman scattering of electrons in quantum wells: identification of elementary excitations *Phys. Rev. B* **73** 235320
[44] Ullrich C A and Vignale G 2001 Theory of the linewidth of intersubband plasmons in quantum wells *Phys. Rev. Lett.* **87** 037402
[45] Hauber A and Fahy S 2017 Scattering of carriers by coupled plasmon-phonon modes in bulk polar semiconductors and polar semiconductor heterostructures *Phys. Rev. B* **95** 045210
[46] Luo Y, Zhao G and Wang S 2020 The electron-phonon scattering and carrier mobility in monolayer AsSb *Phys. Chem. Chem. Phys.* **22** 5688–92
[47] Lee D H, Choi S J, Kim H, Kim Y S and Jung S 2021 Direct probing of phonon mode specific electron-phonon scatterings in two-dimensional semiconductor transition metal dichalcogenides *Nat. Commun.* **12** 4520
[48] Faist J 2007 Wallplug efficiency of quantum cascade lasers: critical parameters and fundamental limits *Appl. Phys. Lett.* **90** 253512
[49] Tame M S, McEnery K R, Özdemir S K, Lee J, Maier S A and Kim M S 2013 Quantum plasmonics *Nat. Phys.* **9** 329–40
[50] Basov D N, Fogler M M and García de Abajo F J 2016 Polaritons in van der Waals materials *Science* **354** aag1992
[51] Brongersma M L, Halas N J and Nordlander P 2015 Plasmon-induced hot carrier science and technology *Nat. Nanotechnol.* **10** 25–34
[52] Kim M, Lee J and Nam J 2019 Plasmonic photothermal nanoparticles for biomedical applications *Adv. Sci.* **6** 1900471
[53] Vahala K *et al* 2009 A phonon laser *Nat. Phys.* **5** 682–6
[54] Beardsley R P, Akimov A V, Henini M and Kent A J 2010 Coherent terahertz sound amplification and spectral line narrowing in a stark ladder superlattice *Phys. Rev. Lett.* **104** 085501